View metadata, citation and similar papers at core.ac.uk

brought to you by CORE

provided by Digitale Bibliothek Thüringen

URN (Paper): urn:nbn:de:gbv:ilm1-2011iwk-136:7

56TH INTERNATIONAL SCIENTIFIC COLLOQUIUM
Ilmenau University of Technology, 12 – 16 September 2011
URN: urn:nbn:gbv:ilm1-2011iwk:5

HIGH RESOLUTION SLOPE MEASURING DEFLECTOMETRY FOR THE CHARACTERIZATION OF ULTRA-PRECISE REFLECTIVE X-RAY OPTICS

F. Siewert[1], J. Buchheim[1], T. Höft[1], S. Fiedler[2], G. Bourenkov[2], M. Cianci[2], R. Signorato[3]*

[1] Helmholtz Zentrum Berlin / BESSY-II, Institut für Nanometer Optik und Technologie
Albert-Einstein-Str. 15, 12489 Berlin, Germany
[2] EMBL Hamburg c/o DESY, Notkestr. 85, 22603 Hamburg, Germany
[3] Bruker ASC GmbH, Friedrich-Ebert-Str. 1. 51429 Bergisch-Gladbach, Germany

ABSTRACT

Slope measuring deflectometry has become a standard technique for the inspection of ultra-precise reflective optical elements for synchrotron applications. We will report on the inspection of ultra-precise adaptive synchrotron mirrors (bimorph mirrors) to be used under grazing incidence condition. The measurements were performed at the BESSY-II Optics Laboratory (BOL) of the Helmholtz Zentrum Berlin (HZB) by use of the Nanometre Optical Component Measuring Machine (NOM). The data obtained by the optical measurements are used to simulate the characteristics of the achievable X-ray focus by ray tracing calculations hereafter demonstrated for the case of the bimorph mirrors of the EMBL MX1 beamline for macromolecular crystallography at the PETRA III synchrotron at DESY (Hamburg).

Index Terms – X-Ray Optics, Synchrotron Optics, Metrology, Bimorph Mirror, Adaptive Optics, NOM, Slope Error,

1. INTRODUCTION

In order to benefit from the high brilliance of state of the art synchrotron sources like 3rd generation storage rings or laser like sources like Free Electron Lasers (FEL) ultra-precise optical elements are required to guide and focus the X-rays beam produced by such state-of-the-art accelerators. Due to the use under grazing incidence condition [1, 2], typical X-ray photon delivery systems (beamlines) are at least 25-35 meter long (for VUV and soft X-ray applications) [3] like at the BESSY-II storage ring of the Helmholtz Zentrum Berlin and have a length of up to 100m and longer (for hard-X-rays) at the PETRA III source at DESY (Hamburg) [4]. Proposed future beamlines for FEL application will even have an overall length of 1km and longer [5] (as planned for the European XFEL in Hamburg). The transport and focusing of photons from such a highly brilliant source to a well defined focal spot without significant loss of brilliance and coherence is an extremely challenging task in X-ray optics and requires optical elements of utmost accuracy and stability. In some cases steering plane mirrors of up to 1000 mm in length with residual figure deviation as low as 2-3 nm peak-to-valley (pv) are required [6].

In the X-ray domain, focusing mirrors are often arranged in a so called Kirkpatrick-Baez (KB) configuration [7]. In order to achieve diffraction limited focusing, hard X-ray mirrors should reach a residual figure error as small as 1 nm rms. The high spatial frequency error requires a micro-roughness of < 0.2 nm rms. This outstanding level of accuracy and finish has been only recently achieved and only for fixed focus mirrors[8]. If tunability in focusing is desired - thus requiring the capability to actively modify the shape of the focusing mirrors - 3 to 5 times higher values for the figure error are the current state-of-the art.

The metrology used to characterize the optics is a limiting factor to manufacture such demanding optical elements [9, 10]. To apply active or adaptive shape control, with mechanical bending (using motorized pushers) or bimorph mirrors (using piezoelectric elements embedded in the mirror itself) to enable a defined shaping of the X-ray beam is a possible approach to optimize the beam transport, specially if some degree of tunability in the position of the focal spot is required. Clearly, apart from the outstanding figure specification the alignment and mounting of such ultra-precise optical elements is a critical and performance limiting factor, too [11].

The accurate off-line characterization of the bendable optical elements is of importance to minimize the effort required to tune them at the X-ray beamline and thus allows the end-user of the optics to achieve rapidly and efficiently the optimal performance of their mirrors. Since the late 1980th the use of high resolution slope measuring deflectometry became a standard technique to measure the quality of reflective X-ray optics for synchrotron [12, 13, 14] as well as for astronomy applications [15]. Moreover, the

principle of slope measuring deflectometry is well established as the national reference for flatness in Germany by use of the Extended Shear Angle Difference method (ESAD) [16, 17] under operation at the Physikalisch Technische Bundesanstalt (PTB). The use of high resolution slope measuring deflectometry as applied for the operation of dedicated optical profilers like the Nanometer Optical Component Measuring Machine (NOM) [18, 19] enables to measure such optics with the required accuracy.

2. THE PRINCIPLE OF SLOPE MEASUREMENT

Systems like the Long Trace Profiler (LTP) [12, 13] or an autocollimator as used in the NOM [18, 19] enable the inspection of reflective surfaces by a direct measurement of the deflection angle of a laser beam. In contrast to interferometry these instruments do not rely on external references. A laser test beam is traced over the sample along the line of inspection. Depending on the local topography the test beam will be reflected into the position sensitive detector of the sensor. The position of the reflected test beam on the CCD-line of the sensor is directly related to the local surface slope, see Figure 1.
The reflection of the test beam along the optical axis of the instrument is determined by the angle θ between the mirror normal and the direction of the impinging laser beam [20, 21]. Than the slope σ is given by:

$$\sigma(x) = \tan\theta = dy/dx \quad . \qquad (1)$$

The relative slope change is measured by scanning along the line of inspection. The sensor detects the change of the angle of reflection from one position x on the substrate to the next position x + Δ x. Figure 1 shows the optical setup for the scanning pentaprism configuration by use of an autocollimator as sensor at the NOM. The topography profile $h(x_k)$ is extracted by spatially integration of the slope data:

$$h(x_k) = h(x_0) + \sum_{m=1}^{k} \frac{dx}{2}\left[\sigma(x_m) + \sigma(x_{m-1})\right] \quad . \qquad (2)$$

Figure 2 gives an example for a slope measurement on a spherical test mirror (R = 9.313 m) and the related profile of height (scan-length = 118mm). Improved integration algorithms such as spline interpolation became an option to handle more noisy data as well [22]. An important criterion for the quality of optical elements is the residual slope and figure error. These information is gained by subtraction of an ideal profile e.g. a circle or an elliptical fit. Figure 3 shows the profile of residual height for the test mirror in a comparison of NOM and LTP measurements. The LTP-measurement was performed at the synchrotron facility SOLEIL (F) [23]. The agreement of both measurements is 1.8 nm pv / 0.4 nm rms for the residual height.

Optical systems up to a length of 1600mm in length can be aligned for inspection at the NOM. The maximum possible scan length of the instrument is 1200mm. A Y-table at the NOM allows a mapping of a surface under test line by line up to 1000mm in length and 300mm width [24]. The spatial period range covered by NOM is from 2mm to the aperture

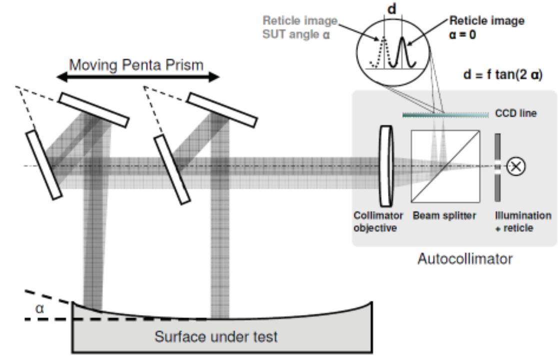

Figure 1. Principle set-up of a scanning mirror based pentaprism slope measuring profiler with an autocollimator detector

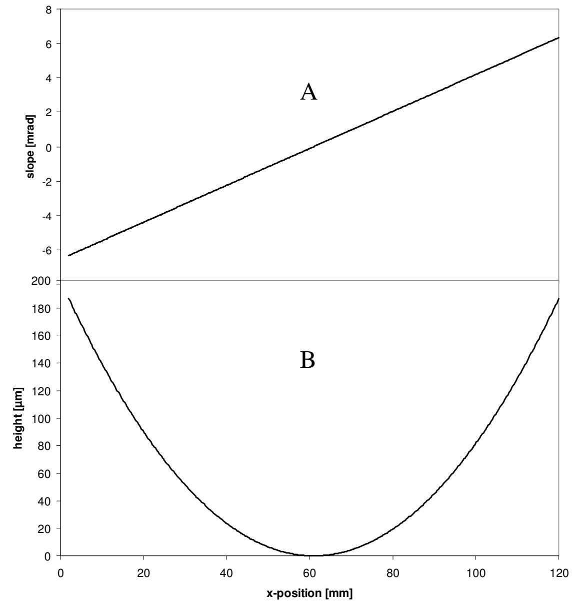

Figure 2: A: profile of slope along a measurement- trace on a spherical test mirror (R=9.313m) and B: the corresponding profile of height

length. Virtually any continuous curved, reflective optical shape can be measured as long as the slope change is within a ± 6mrad acceptance angle. Stitching techniques can be applied in case a long optical surface of significant curvature needs to be measured [25]. It is also noted here that a careful characterization and calibration of the instrument in use is essential to achieve the required measurement performance [26, 27, 28].

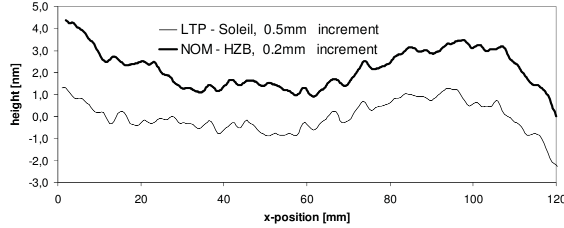

Figure 3: Profile of residual height on the spherical test mirror (R=9.3m) - comparison of NOM and LTP measurements (courtesy of Mouriel Thomasset (Synchrotron SOLEIL) for the LTP-data)

3. ACCURACY REQUIREMENTS FOR GRACING INCIDENCE X-RAY OPTICS

Different types of spatial figure error, characterized by their wavelength (periodicity) on the mirror surface, cause specific contributions on the performance of an X-ray optical system. The high spatial frequency error (HSFE, 1 μm^{-1} – 10 nm^{-1}) causes wide angle scattering typically outside the image field and thus contribute to a decrease of the overall reflectivity. Their contribution can be removed by using suitably placed beam defining slits and cleanup apertures. On the other hand,mid spatial frequency errors (MSFE, 1 mm^{-1} – 10 μm^{-1}) cause an angular spreading down to the small angle scattering range which may even lie inside the image field. Thus e.g. the contrast of the image, also known as Strehl ratio, is reduced. Both error parts are commonly specified in terms of micro-roughness. A state of the art surface finishing of today for X-ray mirrors shows values for both (HSFE and MSFE) of < 0.2 nm rms (measured by use of a white light interferometer).

Whilst HSFE and MSFE are typically described with a statistical approach, a simple geometric approach can be used to describe the impact of mirror shape imperfections on the imaging performance of a X-ray optical system for the low spatial frequency error (LSFE - from full aperture length to 1mm^{-1}) – see Figure 4. This approach is valid for an incoherent incoming X-ray wavefront and for focusing systems that are not operating close to the diffraction limit, where a more sophisticated approach based on wave-optics simulation is required. Within the simplified geometrical approach, a shape deviation of Δh on the

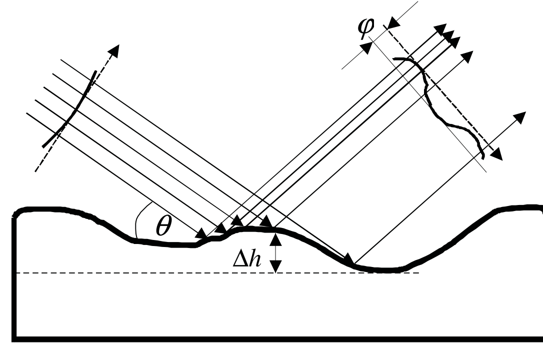

Figure 4: Wave front distortion caused by shape deviations on an imperfect mirror

mirror surface will have an influence on the wave front of a phase φ described as follows:

$$\varphi = \frac{2\Delta h \sin\theta}{\lambda} \tag{3}$$

with θ being the angle of incidence and λ the wave length of the X-ray beam [9].

4. BIMORPH MIRRORS

The main advantages of adaptive bimorph mirrors when compared to either fixed shape or mechanically bent mirrors is their capability to change their overall curvature and also to enable adaptive zonal control of their surface, giving to the user the possibility to act locally on the reflecting surface, down to a length of a few centimeters . A peculiarity of adaptive bimorph mirrors is that the bending mechanism is intrinsic to the mirror itself. Bimorphs are assembled by gluing together two pairs of bilayers consisting of an active element, lead zirconate titanate (PZT) ceramic, and a neutral Silicon or fused silica plate which is then polished. Figure 5 shows an example of a bimorph mirror with 16 piezo- electrodes.

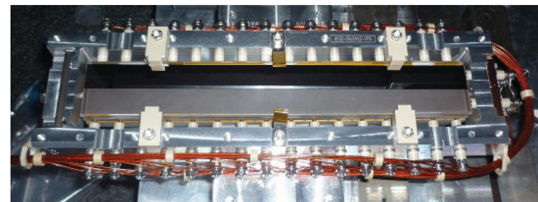

Figure 5: Photograph of a bimorph mirror (MX1-VFM) with 16 piezo electrodes and 2 aperture sections, one Rh-coated and one uncoated. Mirror substrate Fused silica.

The two PZT ceramics are polarised normal to their surface and are assembled in such a way that their polarisation vectors are parallel. A thin driving gold electrode (El_D) is deposited at the PZT-PZT bonding

interface. The ground electrode (El_G) is situated at each of the two ceramic/plate interfaces. When a driving voltage is applied at El_D one PZT shrinks while the other expands. This differential expansion results in a bending of the whole assembly (for more details see literature e.g. [30, 31, 32]).

5. 5. CHARACTERIZATION OF BIMORPH-MIRRORS

It is planned to equip the hard X-ray canted beamlines MX1/MX2 at the PETRAIII storage ring with a set of two bimorph KB focusing mirrors pairs. To guarantee the desired beamline performance these mirrors need to be inspected and carefully characterized by optical metrology before their installation at the beamline.

Thus an acceptance test was performed with the NOM of the HZB. As an example we will describe the mirror tuning procedure for the vertical focusing mirror MX1-VFM. It is a mirror of 298 mm in length and 45 mm in width with 16 equi-spaced driving electrodes deposited on the PZT ceramics, thus allowing to steer the reflective surface locally with a meridional resolution of slightly more than 15 mm (Figure 5). The useful optical aperture length is 250 mm. The micro-roughness of that mirror of <0.2 nm rms was measured by use of a white light interferometer Micromap Promap (magnification 20x).

The tuning of the mirror is based on the determination of the so-called “interaction matrix”, which describes the reaction of the reflecting surface to individual, known pulses sent to each of the 16 electrodes. Then, using appropriate matrix inversion algorithms the interaction matrix is inversed to obtain the so-called “control matrix” that allows driving the mirror to a desired shape in a deterministic and accurate way as it takes into account all the cross-correlation between the electrodes. For a detailed description of the interaction-control matrix method, please refer to ref [30, 31].

The interaction-control matrix method requires a series of regular, repeated measurements and is thus very well suited for being automated. A LabVIEW©-based routine was applied to link the NOM controls with the bimorphmirror High Voltage Bipolar Power Supply (HVBPS); this allows a direct communication of both systems and automatic measurements as it synchronizes the NOM scans with the required voltage pulses. It takes about 6 hours to determine the whole set of 16 pulse functions. A relaxation time of 20 min after setting a voltage to an electrode was used to ensure that the mirror had stabilized physically. The setting of the desired voltage takes a few minutes required by the creep/hysteresis minimization procedures. Eventually, a set of of 17 (n+1) slope profiles recorded along the meridional direction of the mirror allows to extract the 16 individual pulse functions of the 16 (n) electrodes. The option of automatic measurements allowed to collect the matrix data overnight (11pm – 5am). This option is providing excellent environmental conditions due to a low level of cultural noise and thus a lower vibration level during the measurement in general. A climate machine in the laboratory enables a thermal stability of 5mK/h.

Figure 6 shows the 16 individual pulse functions in terms of height change along the meridional mirror axis obtained for the mirror MX1-VFM. A software tool allows uploading the individual matrix data-set to the HVBPS controller in order to optimize the mirror in terms of minimizing its figure error with respect to the target elliptical shape. The final optimized state is usually achieved after 3 iterations of shape improvement, (see chapter 6).

6. MEASUREMENT RESULTS

Figure 7 and 8 show the results for the optimization achieved for the MX1-VFM. The optimized state of the mirror shows a residual figure error of 2.8 nm rms / 13 nm pv after three iterations of shape optimization, compared to 22.4 nm rms / 68 nm pv initially. The achieved residual figure error of 2.8 nm rms corresponds to a residual slope error of 0.44 µrad rms and shows that the mirror is compliant with the specification of 0.5 µrad rms. The horizontally focusing mirror MX1-HFM is a mirror of 448 mm length and 45 mm width. The useful optical length is 400 mm. A factor of three improvement in shape error was achieved after 3 iterations. The MX1-HFM was initially characterized by a residual figure error of 20.6 nm rms / 76 nm pv – finally 5.6 nm rms / 24 nm pv was achieved – see Figure 10. This result corresponds to a residual slope error of 0.58 µrad rms (see Figure 9). For the centre section of the aperture (from x = 80 to 350) a residual slope error of 0.36 µrad rms is achieved.

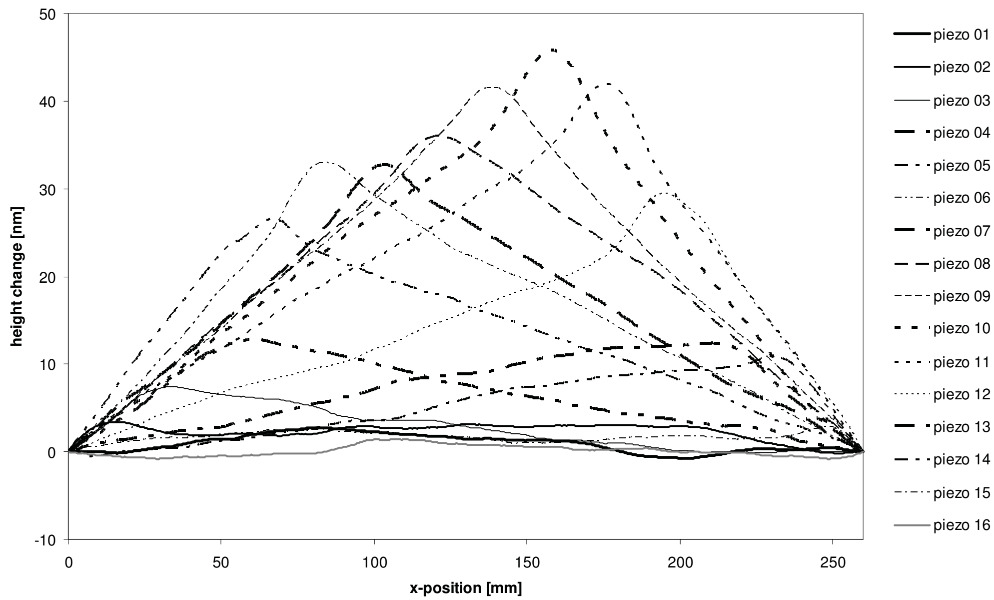

Figure 6: Electrodes pulse functions for the MX1-VFM bimorph mirror, showing the effect of applying a 50 V pulse to each piezo element in turn. The data shows that the piezos can deliver a figure control in the nanometre range, as the input voltage can be controlled with sub-Volt accuracy.

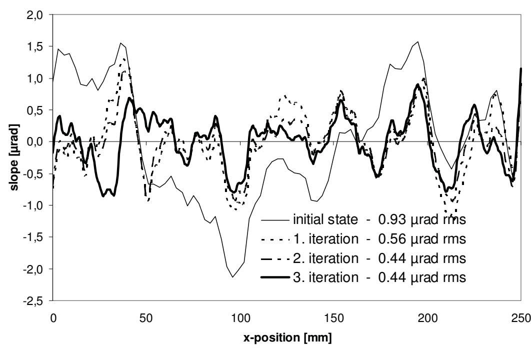

Figure 7: profile of residual slope error for different states of the vertical focussing mirror MX1-VFM, finally a state of 0.44 µrad rms is achieved

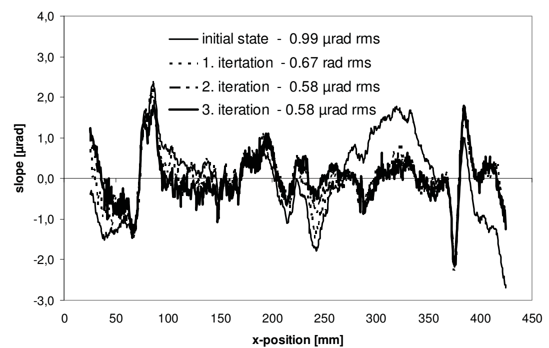

Figure 9: profile of residual slope for different states of the horizontal focussing mirror MX1-HFM, finally a state of 0.58 µrad rms is achieved

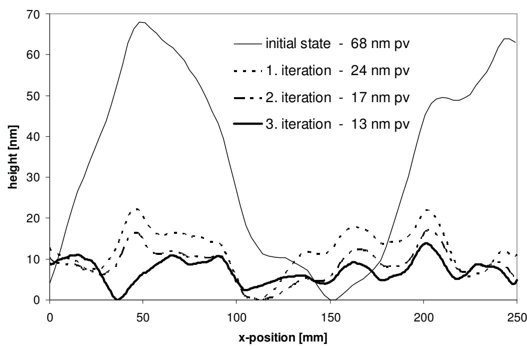

Figure 8: profile of residual height error for different states of the vertical focussing mirror MX1-VFM, finally a state of 2.8 nm rms / 13 nm pv is achieved

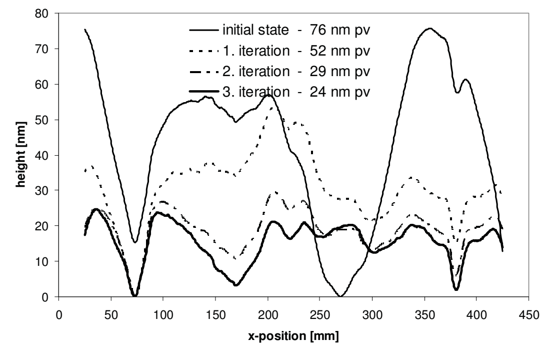

Figure 10: profile of residual height for different states of the horizontal focussing mirror MX1-HFM, finally a state of 5.6 nm rms / 24 nm pv is achieved

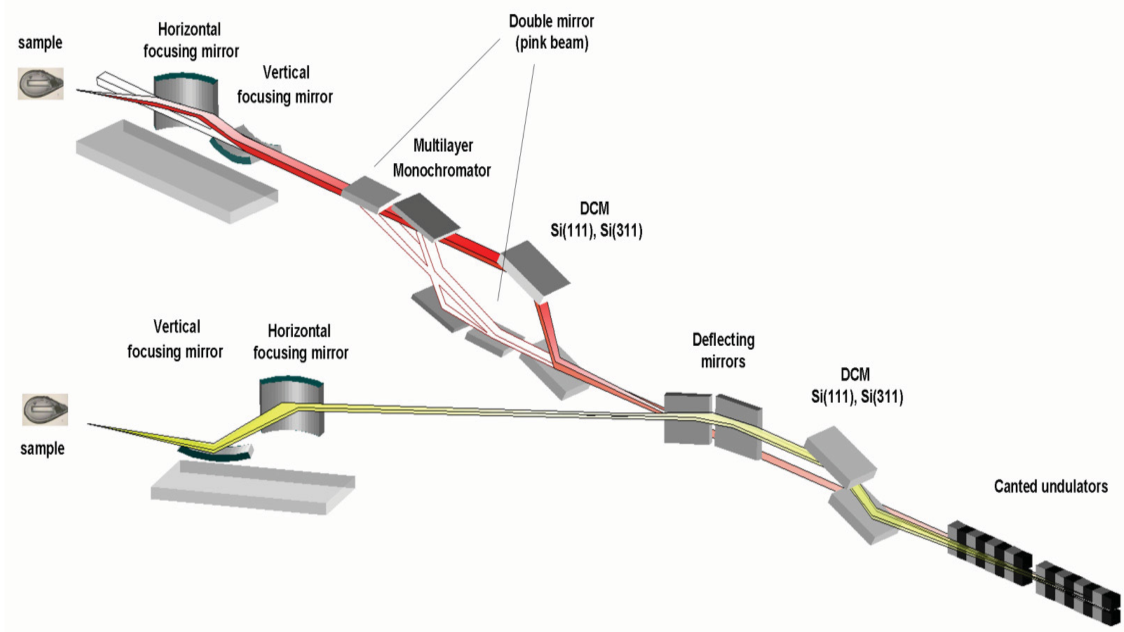

Figure 11: Optical layout of EMBL beamlines for macromolecular crystallography, MX1 and MX2, at PETRA III / DESY in Hamburg.

7. BEAMLINE MX1/MX2 AT PETRA III

The two EMBL beamlines for macromolecular crystallography at PETRA III, MX1 and MX2, are situated on the same straight section of the storage ring. They receive their radiation from two identical undulators canted by 5 mrad to each other. The basic optical layout of the beamlines is very similar (Figure 11). A fixed exit double Si111 crystal monochromator defines the energy bandwidth and a KB adaptive bimorph mirror set in front of the experiment focuses the beam in vertical and horizontal direction. The beamlines differ mainly in their de-magnification ratios determined by the source-to-mirror distance and mirror-to-focus distance (MX1 [horizontal / vertical]: 1: 12 / 1:13; MX2: 1:60 / 1:41). In the MX1 beamline, additionally a horizontal deflecting mirror set is installed upstream the KB optics to increase the angular offset of the two beamline to 21 mrad.

8. BEAMLINE PERFORMANCE SIMULATIONS

To evaluate the expected beamline performance ray tracing simulations were performed. First, the ray distribution in the source has been modelled using the SHADOW code [33]. We applied standard parameters of the storage ring and of the 2m long U28 undulator at the high-beta section [34] on the input side. Within the energy band width of the MX1 beamline, and within the angular acceptance of the KB system, joint distribution of ray positions and directions in either the vertical or horizontal direction were indistinguishable from the bivariate Gaussian; position and direction at the source do not correlate. This permits to evaluate the X-ray intensity profile in the focus analytically using measured slope errors. Probability $p(z)$ to observe a ray at a distance z (vertical or horizontal) from the optical axis in the focal plane is expressed by:

$$p(z) \propto \sum_m \exp\left[-\frac{1}{2}\left(\left(\frac{x_m\theta}{p\sigma'_z}\right)^2 + \left(\frac{2\varepsilon_m q - z}{\sigma_z \, q/p}\right)^2\right)\right].$$

Here, σ_z and σ'_z are the rms. source size and divergence in z-direction respectively, p is the distance from the source to the mirror, q is the distance from mirror to the focus, θ is a grazing angle. m indexes the measurement point of the slope error ε_m at the distance x_m from the center of the mirror. The above equation was derived under simplifying assumptions that $\sigma_z << p\sigma'_z$, and that the mirrors length $L << q < p$. The assumptions hold for the MX1 geometry. In this form, the equation expresses the intensity distribution in focus as a convolution of slope error distribution with the de-magnified source (the second term under exponential),

weighted by the beam intensity distribution across the mirror (the first term).

The beam profiles calculated using the parameters indicated in Table 1 are shown in figures 12 and 13 for horizontal and vertical focus, respectively. In horizontal direction, the HFM shape optimization reduces the FWHM source size from 38 to 28 µm. The features due to mirror figure are smeared in focus due to the large source size.

In the vertical direction, the simulation predicts that the VFM in its initial state provides multimodal beam that is hardly usable for precision crystallographic experiments. This is clearly due to the small vertical source size. We expect that a number of factors related to the storage ring, undulator and upstream beamline optical elements will increase the effective source size at MX1. In the absence of experimental measurements of the effective source size, we carried out the calculations applying fudge factors 2 and 4 to the theoretical one (i.e. σ_z = 11 µm and 22 µm on Fig. 13b and 13c respectively). Even under these assumptions the shape of the 'initial state' vertical focus is unacceptable. For optimized mirror figure fairly smooth and well useable vertical profiles are predicted under realistic assumptions on the source size.

Table 1. MX1 parameters used in ray tracing calculations

	Vertical	Horizontal
σ_z, [µm]	5.4	127
σ'_z, [µrad]	4.5	8.8
p, [m]	53.250	52.750
q, [m]	4.000	4.500
θ, [mrad]	3.0	3.0

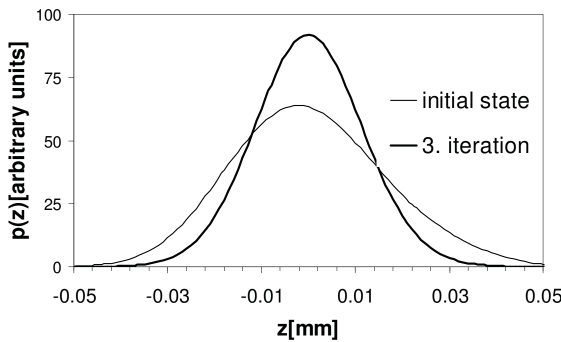

Figure12. Simulated intensity distribution in the horizontal focus.

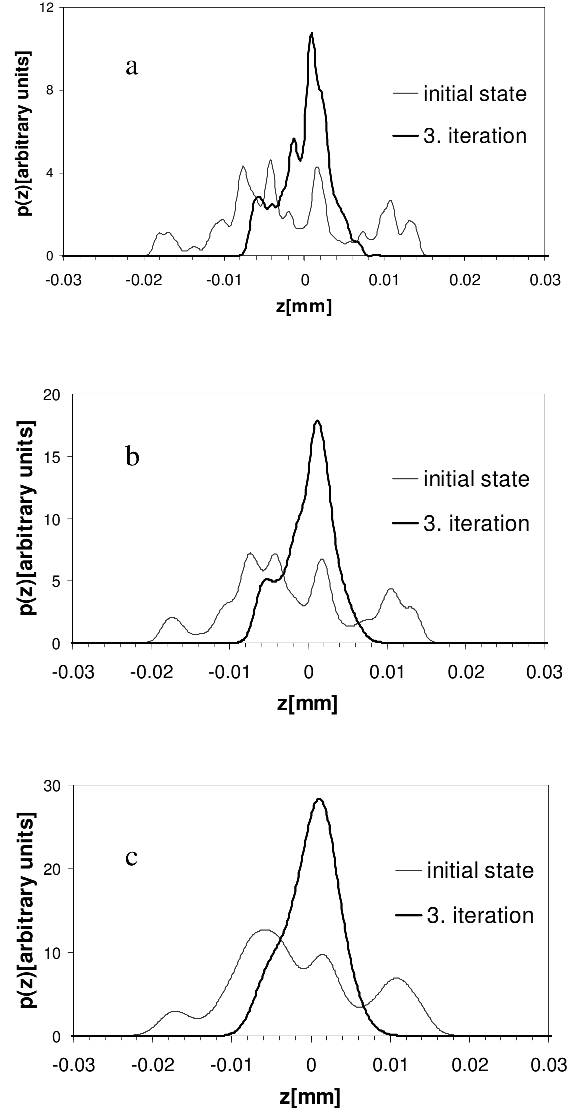

Figure 13. Simulated intensity distribution in the vertical focus for theoretical source size (a), theoretical source size fudged by a factor 2 (b), and by a factor 4 (c).

9. CONCLUDING REMARKS

We have shown slope measuring deflectomety as a power full method for the characterization of ultra-precise reflective X-ray optical elements. The described method enables adaptive optical elements, like bimorph-mirrors, to be precisely inspected by use of the BESSY-NOM and thus allows to be optimized in shape by a factor of 4-5 to a residual figure error of 10 to 20 nanometer about. The off-line metrological measurements of the mirrors have been demonstrated to be used to simulate the expected performance in the optical system (beamline).

10. ACKNOWLEDGEMENTS

The authors like to thank Mouriel Thomasset Synchrotron Soleil (F) for providing the LTP-data on the calibration sphere,

11. REFERENCES

[1] Hans Wolter, *Spiegelsysteme streifenden Einfalls als abbildende Optiken für Röntgenstrahlen*, Annalen der Physik, 6. Folge Bd.10, 1952

[2] M.R.Howells, *Mirrors for Synchrotron Radiation Beamlines*, New Directions in Research with Third-Generation Soft X-Ray Synchrotron Radiation Sources, LBL-34750/UC-406, Maratea, 1992

[3] R. Follath, J.S. Schmidt, F. Siewert et all., *Commissioning of the U49/2-PGM1 beamline*, AIP Conference Proceedings, Vol. 705, 348-351pp, Mellville, NY, 2004

[4] E. Weckert, K. Balewski, W. Brefeld, W. Decking, W. Drube, H. Franz, P. Gürtler, U. Hahn, J. Pflüger, H. Schulte-Schrepping, M. Tischer and J. Schneider, *PETRA III: A New High Brillance Synchrotron Radiation Source at DESY*, AIP Conference Proceedings, Vol. 705, pp **73-76**, Mellville, NY, 2004

[5] M. Altarelli et all., The European X-Ray Free Electron Laser – Technical Design Report, DESY, Hamburg, July 2006

[6] L. Samoylova, H. Sinn, F. Siewert, H. Mimura, K. Yamauchi, T. Tschentscher, *Requirements on hard x-ray grazing incidence optics for European XFEL: analysis and simulation of wavefront transformations*, Proc. of the SPIE, Vol. 7360, Bellingham, WA, 2009

[7] P. Kirkpatrick and A.V. Baez*, Formation of Optical Images by X-Rays*, JOSA, Vol. 38 No. 9, 1948

[8] F. Siewert, J. Buchheim, S. Boutet, M.G.J. Williams, P. Montanez, J. Krzywinski, R. Signorato, *The first diffraction limited hard X-ray KB-focussing mirror pair for the Linac Coherent Light Source – high resolution slope measuring deflectometry for ultra-precise mirror characterization*, under preparation

[9] H. Mimura, S. Handa, T. Kimura, H. Yumoto, D. Yamakawa, H. Yokoyama, S. Matsuyama, K. Inagaki, K. Yamamura, Y. Sano, K. Tamasaku, Y. Nishino, M. Yabashi, T. Ishikawa, K. Yamauchi, *Breaking the 10 nm barrier in hard-X-ray focusing*, Nature Physics 1457, 2009

[10] H. Thiess, H. Lasser, F. Siewert, *Fabrication of X-ray mirrors for synchrotron applications*, Nucl. Instr. and Meth. A, Volume: 616 Issue: 2-3 pp157-161 Published: 2010

[11] F. Siewert, J.Buchheim, T. Zeschke, G. Brenner, S. Kapitzki, K. Tiedtke, *Sub-nm accuracy metrology for ultra-precise reflective X-ray optics*, Nucl. Instr. and Meth. A, Volume: 635, pp52-57 Published: 2011

[12] P. Takacs, S. N. Qian and J. Colbert, *Design of a long trace surface profiler*, Proc. of SPIE Vol. 749, Bellingham, WA, 1987, pp. 59-64

[13] P. Takacs, S. N. Qian, *Surface Profiling interferometer*, US patent No.U4884697, Dec. 5, 1989

[14] S.C. Irick, W.R. McKinney, *Advancements in One-Dimensional Profiling With a Long Trace Profiler*, Proc of Int. Symp. on Optical Fabric Testing and Surface Evaluation, Tokyo, 1992

[15] M. Gubarev, T. Kester, P.Z. Takacs, *Calibration of a vertical-scan long trace profiler at MSFC*, “Optical Manufacturing and Testing IV”, ed H. Philip Stahl, Proc. of SPIE 4451, Bellingham, WA, 2001I.

[16] Weingärtner, M. Schulz, C. Elster, *Novel scanning technique for ultra-precise measurement of topography*, “Optical Manufacturing and Testing III”, Proc. of SPIE Vol. 3782, Bellingham, WA, 1999

[17] R.D. Geckeler, I. Weingärtner, *Sub-nm topography measurement by deflectometry: flatness standard and wafer nanotopography*, Proc. of SPIE, 4779, Bellingham, WA, 2002, pp. 1-12

[18] Frank Siewert, Tino Noll, Thomas Schlegel, Thomas Zeschle and Heiner Lammert, *The Nanometer Optical Component Measuring Machine: a new Sub-nm Topography Measuring Device for X-Ray Optics at BESSY*, AIP Conference Proceedings, Vol. 705, pp 847-850, Mellville, NY, 2004

[19] S.G. Alcock, K.J.S. Sawhney, S. Scott, U. Pedersen, R. Walton, F. Siewert, T. Zeschke, T. Noll and H. Lammert, *The Diamond-NOM: A non-contact profiler capable of characterizing optical figure error with sub-nm repeatability*, Nucl. Instrum. Meth. A 616 (2010) pp224-228

[20] S.C. Irick, Rev. Sci. Instrum 63(1), 1992

[21] F. Siewert, *Slope Error and Surface Roughness*, in: Modern Developments in X-ray and Neutron Optics, Springer 2008

[22] G. Ehret, M. Schulz, M. Stavridis, C. Elster, *A new flatness reference measurement system based on deflectometry and difference defelctometry*, in Fringe 2009: 6th International Workshop on Advanced Optical Metrology, W. Osten, M. Kujawinska eds, 318-323 (Springer-Verlag, Berlin 2009)

[23] M. Thomasset, S. Brochet, F. Polack, *Latest metrology results with the SOLEIL synchrotron LTP*, in Advances in Metrology for X-Ray and EUV Optics edited by Lahsen Assoufid, Peter Z. Takacs, John S. Taylor, Proc. of SPIE, Vol. 5921-01, Bellingham, WA, 2005, DOI: 10.1117/12.621073

[24] F. Siewert, H. Lammert, T. Noll, T. Schlegel, T. Zeschke, T. Hänsel, A. Nickel, A. Schindler, B. Grubert, C. Schlewitt, *Advanced metrology: an essential support for the surface finishing of high performance x-ray optics*, in Advances in Metrology for X-Ray and EUV Optics edited by Lahsen Assoufid, Peter Z. Takacs, John S. Taylor, Proc. of SPIE, Vol. 5921-01, Bellingham, WA, 2005, DOI: 10.1117/12.622747

[25] F. Polack, M. Thomasset, S. Brochet, A. Rommeveaux, *An LTP stitching procedure with compensation of instrument errors: Comparison of SOLEIL and ESRF results on strongly curved mirrors*, , Nucl. Instrum. Meth. A 616 (2010) 207-211
[26] V. Yashchuk, W. McKinney, T. Warwick, T. Noll, F. Siewert, T. Zeschke, R. Geckeler, *Proposal for a Universal Test Mirror for Characterization of Slope Measuring Instruments*, Advances in Metrology for X-Ray and EUV Optics II, Proc. of SPIE, Vol. 6704, Bellingham, WA, 2007
[27] F. Siewert, J. Buchheim, T. Zeschke, *Characterization and calibration of 2nd generation slope measuring profiler*, Nucl. Instr. And Meth. A (2010), doi: 101016/J.nima.2009.12.033
[28] R.D. Geckeler, A. Just, M. Krause, V.V. Yashchuk, *Autocollimators for deflectometry: Current status and future progress*, Nucl. Instrum. Meth. A 616 (2010) 140-146
[29] A. Schindler, T. Haensel, A. Nickel, H. Lammert, F. Siewert, *Finishing procedure for high performance synchrotron optics*, Optical Manufacturing and Testing V, Book Series: Proceedings of SPIE, Volume: 5180 pp: 64-72 Published: 2003
[30] J. Susini, D, Labergerie; L. Zhang, *Compact active/adaptive x-ray mirror: Bimorph piezoelectric flexible mirror*, Rev. Sci. Instrum. 66 (2), February 1995
[31] R. Signorato. O. Hignette, J. Goulon, *Multidegmented piezoelectric mirrors as active/adaptive optics components*, Journal of Synchrotron Radiation, Vol. 5, pp 797 – 800, 1998
[32] R. Signorato, D. Häusermann, M. Somayazulu, J.F. Carre, Performance o fan adaptive µ-focussing Kirkpatrick-Baez system for high pressure studies at the Advanced Photon Source, Proc. of SPIE Vol. 5193, Bellingham, WA, 2004
[33] C. Welnak, G. Chen and F. Cerrina, SHADOW: a synchrotron radiation and X-ray optics simulation tool, Nucl. Instr. Methods A, 347, pp: 344-347 (1994)
[34] Balewski et al., PETRA-III, A Low Emittance Synchrotron Radiation Source – Technical Design Report, DESY, Hamburg (February 2004)